HHS Public Access

Author manuscript

Nano Lett. Author manuscript; available in PMC 2019 April 15.

Published in final edited form as:

Nano Lett. 2018 December 12; 18(12): 7590–7600. doi:10.1021/acs.nanolett.8b03149.

Modifying a commonly expressed endocytic receptor retargets nanoparticles *in vivo*

Cory D. Sago[#1], **Melissa P. Lokugamage**[#1], **Gwyneth N. Lando**[1], **Naima Djeddar**[2], **Nirav N. Shah**[3], **Chris Syed**[1], **Anton V. Bryksin**[2], and **James E. Dahlman**[1]

[1]Wallace H. Coulter Department of Biomedical Engineering, Georgia Institute of Technology, Atlanta GA, 30332, United States of America

[2]Parker H. Petit Institute for Bioengineering and Bioscience, Georgia Institute of Technology, Atlanta GA, 30332, United States of America

[3]School of Biological Sciences, Georgia Institute of Technology, Atlanta GA, 30332, USA

[#] These authors contributed equally to this work.

Abstract

Nanoparticles are often targeted to receptors expressed on specific cells, but few receptors are (i) highly expressed on 1 cell type and (ii) involved in endocytosis. One unexplored alternative is manipulating an endocytic gene expressed on multiple cell types; an ideal gene would inhibit delivery to cell type A more than cell type B, promoting delivery to cell type B. This would require a commonly expressed endocytic gene to alter nanoparticle delivery in a cell type-dependent manner *in vivo;* whether this can occur is unknown. Based on its microenvironmental regulation, we hypothesized Caveolin 1 (Cav1) would exert cell type-specific effects on nanoparticle delivery. Fluorescence was not sensitive enough to investigate this question, and as a result, we designed a platform named QUANT to study nanoparticle biodistribution. QUANT is 10^8x more sensitive than fluorescence and can be multiplexed; by measuring how 226 lipid nanoparticles (LNPs) delivered nucleic acids to multiple cell types *in vivo* in wildtype and Cav1 knockout mice, we found Cav1 altered delivery in a cell-type specific manner. Cav1 knockout did not alter LNP delivery to lung and kidney macrophages, but substantially reduced LNP delivery to Kupffer cells, which are liver resident macrophages. These data suggest caveolin-mediated endocytosis of nanomedicines by macrophages varies with tissue type. These results suggest manipulating receptors expressed on multiple cell types can tune drug delivery.

Keywords

DNA barcode; nanoparticle; drug delivery; Caveolin; Kupffer cell; ddPCR

Correspondence: james.dahlman@bme.gatech.edu.

Author contributions. C.D.S., M.P.L., and J.E.D. designed experiments, which were performed by C.D.S., M.P.L., G.N.L., N.D., N.S, A.V.B., and J.E.D. C.D.S, M.L, N.S, and J.E.D. analyzed data. C.D.S., M.P.L., and J.E.D. wrote the paper, which was reviewed by G.N.L., N.D., N.S., and A.V.B.

Competing interests. C.D.S., M.P.L., and J.E.D. have filed for intellectual property related to material within this publication.

Data and materials availability. The data, analyses, and scripts used to generate all figures in the paper are available upon requests made to dahlmanlab.org.

Introduction.

siRNAs delivered to hepatocytes have treated disease in patients[1–3], but delivery to other cell types remains challenging[4]. The liver exhibits physiological advantages that promote nanoparticle accumulation[5, 6], and as a result, rational approaches will be required to minimize unwanted liver delivery. An ideal approach would involve (i) synthesizing hundreds of nanoparticles with diverse chemical structures, and (ii) analyzing them *in vivo* using an animal model that (iii) tests a specific biological hypothesis (e.g., gene X alters delivery) *in vivo*. However, the current gold standard is to study nanoparticles *in vitro.* Thousands of nanoparticles can be synthesized for nucleic acid delivery, but they are screened *in vitro*[7–12], which can be a poor predictor of *in vivo* delivery[13]. Genes that alter nanoparticle delivery *in vitro* have been identified[14–17]; genes that affect systemic nanoparticle delivery *in vivo* remain much more difficult to study. Exceptions to this[18–21] have provided valuable insights, but have focused on soluble factors in serum[18, 19] or receptors on hepatocytes[19–21]. Whether a commonly expressed gene can exert cell type-specific effects on nanoparticle delivery *in vivo* remains unexplored.

Nanomedicines are often delivered using ligands that bind receptors expressed on target cells[22]. For example, the asialoglycoprotein receptor (ASGPR) is expressed on hepatocytes; N-acetylgalactosamine conjugates (GalNAc) have targeted ASGPR[23], leading to delivery in animals and patients. Other receptors include epidermal growth factor (EGFR)[24], folate receptor[25], transferrin receptor[26], VCAM-1[27], and ICAM-1[28]. Given that few receptors are (i) highly expressed on one cell type and (ii) induce nanomedicine endocytosis upon binding, we envisioned an alternative approach: manipulating an endocytosis receptor expressed on many cells. An ideal receptor would inhibit delivery to cell type A more than cell type B, promoting delivery to cell type B. This approach is timely. Our understanding of cell heterogeneity is progressing; RNA-seq[29] has revealed that gene expression varies with disease state[30] and within cell populations previously believed to be homogeneous[31, 32]. Large scale approaches like the Human Cell Atlas[33] are likely to uncover endocytic genes whose importance varies with cell type. Since hundreds of genes are in involved in endocytosis[34], and many genes are regulated by disease- and microenvironment-derived cues[35, 36], it is foreseeable that manipulating 1 gene could alter delivery in a tissue- or disease-specific manner. To test the hypothesis that manipulating a commonly expressed receptor can affect nanoparticle delivery in cell type-dependent manner, we focused on Caveolin 1 (Cav1), a gene involved in caveolin-mediated endocytosis[37]. Caveolin can endocytose nanoparticles *in vitro*[38] and *in vivo*[39]. Its expression changes with fibrosis[40–43], lung disease[44], cancer[45–48], neurological disease[49, 50], and other pathologies[51–53], demonstrating that its expression is regulated by microenvironmental signals and disease.

Results.

Given that *in vitro* nanoparticle delivery can be a poor predictor of *in vivo* delivery[13] and that gene expression can change when cells are cultured *in vitro*[54], we tested our hypothesis *in vivo,* eventually testing 226 chemically distinct lipid nanoparticles (LNPs). This approach is distinct from previous studies for 2 reasons. First, LNP studies typically evaluate many

nanoparticles *in vitro* before selecting a small number to test *in vivo*[7–12]. Second, most LNP studies focus on hepatocytes, not macrophages[8–12].

We used microfluidics[55] to formulate a validated ionizable LNP that has delivered siRNAs *in vivo*[7, 56–60]. The LNP carried a single stranded DNA (ssDNA) (**Supplementary Fig. 1a**) that was chemically modified with phosphorothioates to reduce exonuclease degradation, and fluorescently tagged with Alexa-647. We chose Alexa-647 since it was significantly brighter than Alexa488 (**Supplementary Fig. 1b**). One hour after intravenously injecting wildtype (WT) or Cav1 deficient ($Cav1^{-/-}$) mice with the clinically relevant[3] dose of 0.5 mg / kg DNA, we quantified Alexa-647 mean fluorescence intensity (MFI) in 13 cell types (**Supplementary Fig. 1c**) using flow cytometry (**Supplementary Fig. 1d,e**). In WT mice, >75% of the MFI signal was found in Kupffer cells or hepatic endothelial cells; we could not reliably quantify delivery in other cell types. The same was true for $Cav1^{-/-}$ mice, suggesting Cav1 did not change LNP biodistribution (**Supplementary Fig. 1f**).

Given the role of Cav1 in nanoparticle endocytosis[61], the fact caveolin inhibitors affect this LNP *in vitro*[7], and the fact this LNP delivers siRNA and sgRNA to pulmonary and cardiovascular endothelial cells *in vivo*[7, 56–60], we hypothesized that our Alexa-647 biodistribution data were inaccurate. Our hypothesis was recently strengthened by demonstrations that the fluorescent biodistribution of small molecules delivered by nanoparticles can change in ways that do not reflect delivery[62]. Since nucleic acids are degraded by nucleases that cleave phosphodiester bonds[63] - and fluorophores are not – we reasoned the fluorescent signal may not track with the nucleic acid. To test this, we engineered a novel biodistribution assay named QUantitative Analysis of Nucleic acid Therapeutics (QUANT); QUANT utilizes digital droplet PCR (ddPCR) – a technique used to quantify rare genomic events[64] – to quantify the biodistribution of the nucleic acid itself with high sensitivity, allowing us to directly compare it to the biodistribution of the fluorescent readout. This is important since fluorescent biodistribution studies are ubiquitously used throughout to measure nucleic acid biodistribution.

Since ddPCR requires efficient DNA amplification, we rationally designed QUANT DNA barcodes to increase DNA polymerase access (**Fig. 1a,b, Supplementary Fig. 1a**). We minimized DNA 2˚ structure on the forward and reverse primer sites and minimized G-quadruplex formation by separating our randomized 7 nucleotide region[13, 65] into semi-randomized NWNH and NWH sites. We flanked the primer sites with 3 additional phosphorothioate-modified nucleotides to reduce exonuclease degradation of the primer site. Finally, we identified universal primer binding sites that would not amplify mouse or human genomic DNA (gDNA). Specifically, we designed primers with similar melting temperatures (within 1˚C) and added them to human and mouse gDNA without barcode template (**Supplementary Fig. 2a**). We identified primers that did not amplify gDNA after 40 cycles (**Supplementary Fig. 2b**), but amplified barcode templates with 20 cycles. Based on these results, we added the ‘no gDNA background’ primer sites to our barcodes. We then optimized the ddPCR protocol (**Supplementary Fig. 2c-g**) by varying annealing temperatures, primer concentrations, and probe concentrations. We increased the signal: noise ratio 14-fold compared to current standard protocols[64]. As a control, we scrambled the

ddPCR probe site; no signal was generated, demonstrating that the signal required specific barcode-probe interactions (**Supplementary Fig. 2h**).

Standard curve experiments revealed QUANT was highly sensitive. QUANT ddPCR signal was linear (with respect to the DNA added) when barcodes were diluted in Tris-EDTA buffer to a concentration between 750 aM and 12 fM (R^2 = 1.00) and was detected at 300 aM (**Fig 1c, d**). As a control, we reduced the concentration to 30 aM, and did not observe readouts above an untreated baseline. QUANT was also highly sensitive *in vitro*. We fluorescently tagged QUANT barcodes and administered them to immortalized aortic endothelial cells (iMAECs)[66] in 96 well plates with Lipofectamine 2000 (L2K) at doses between 1 pg and 400 ng / well. Twenty-four hours later, we quantified biodistribution using flow cytometry, and observed measurable (but non-linear) increases in MFI above 10 pg / well (**Supplementary Fig. 3a**). Separately, we administered QUANT barcodes without a fluorophore at doses between 60 and 16,000 zeptogram (zg) / well. ddPCR readouts were linear (R^2 = 0.91) between 120 and 8000 zg / well (**Fig. 1e**), $10^8\times$ lower than the minimum dose required for a fluorescent signal. We then formulated QUANT barcodes into validated LNPs[7] using microfluidics[55]; LNPs carrying barcodes formed nanoparticles with an average hydrodynamic diameter of 53 nm. We intravenously administered them at 0.5 mg / kg, isolated lung endothelial cells using fluorescence activated cell sorting (FACS) 24 hours later, and quantified barcode delivery using ddPCR. We compared samples immediately after completing the experiment to samples analyzed after storage at −20˚C for 20 or 31 days. Readouts were consistent when performed by different individuals using different reagent stocks (**Fig 1f**).

We hypothesized that fluorescent biodistribution would yield different results than QUANT. We formulated the same LNP[7] with QUANT barcodes that were, or were not, fluorescently tagged with Alexa-647. One hour after intravenously administering 0.5 mg / kg, we isolated the same 13 cell types (**Supplementary Fig. 1c**) using FACS and quantified LNP delivery using Alexa-647 MFI or QUANT (**Fig. 2a**). 87% of the Alexa-647 signal was found in liver cells; the remaining 10 cell types only generated 13% of the total fluorescent signal (**Fig. 2b-d**). QUANT biodistribution was different; only 56% of the ddPCR signal derived from the liver (**Fig. 2b-d**). We compared delivery in all 13 cell types and found statistically significant differences in 7 of them (**Fig. 2e**). In **Figure 2E**, we normalized delivery to Kupffer cells, which readily clear nanoparticles[5, 6]. Notably, in all cases, fluorescence overestimated liver biodistribution. To exclude the possibility these results were due to a specific timepoint, we performed a pharmacokinetics experiment in 5 cell types: liver endothelial cells, Kupffer cells, hepatocytes, lung endothelial cells, and lung macrophages. We intravenously injected mice with 0.5 mg / kg QUANT barcodes, and sacrificed mice 0.4, 0.75, 1.25, 12, 24, and 36 hours later (**Fig 3a**). At the 0.4, 0,75, and 1.25 hour timepoints, fluorescent biodistribution was localized to liver cells; only 1 of 6 non-liver signals (2 cell types, 3 timepoints) were statistically significant compared to untreated mice. At later timepoints, fluorescent biodistribution was not significantly above PBS-treated mice in any cell type. Out 30 potential data points (5 cell types, 6 time points), only 6 generated a fluorescent signal that was statistically significant compared to untreated mice (**Fig. 3b**). By contrast, QUANT-based biodistribution was observed in all 30 data points (**Fig 3b**). We

calculated under the curve (**Fig. 3c**) and the maximum DNA delivery (**Fig. 3d**); once again, the results suggested Alexa-647 fluorescence overestimated delivery to the liver. Finally, we investigated how robust QUANT readouts were across experiments. We compared the absolute ddPCR values from all 5 cell types in the first QUANT biodistribution experiment (**Fig. 2**) and the pharmacokinetic experiment (**Fig. 3**) at similar timepoints (1 and 1.25 hours, respectively). ddPCR readouts were reproducible (R^2=0.98) between experiments (**Fig 3e**). Figures 1–3 demonstrate that QUANT is a sensitive and repeatable method of quantifying nanoparticle biodistribution.

QUANT enabled us to measure LNP delivery with increased sensitivity; we took advantage of this to test the hypothesis Cav1 affects LNP delivery in a cell type-specific manner *in vivo*. To ensure our results were not specific to 1 LNP chemical structure, we exploited a second advantage of QUANT: it can be multiplexed so the distribution of >100 LNPs is analyzed at once. Multiplexed analysis of nanoparticle delivery has been reported by our group[13, 65] and others[67], but critically, these barcoding systems can only quantify delivery of LNP-1 relative to LNP-2 within the same sample; it cannot quantify absolute delivery. Without the ability to quantify absolute delivery, it is difficult to directly compare readouts (i) between different tissues, (ii) between different mouse models (e.g., WT and Cav1$^{-/-}$), or (iii) between ddPCR and fluorescence.

We performed 2 high throughput *in vivo* LNP screens. We formulated LNP-1, with chemical structure 1, so it carried QUANT barcode 1; we formulated LNP-N, with chemical structure N, to carry QUANT barcode N (**Fig 4a-c**). The 8 nucleotide barcode region on the QUANT DNA sequence - located in the center - can generate 65,536 unique barcodes; we designed 156 that were compatible with one another on Illumina sequencing machines (**Supplementary Fig. 4a**). Each barcode has a base distance of 3 or more, which means every 8 nucleotide barcode sequence is different from all other 8 nucleotide barcode at 3 of the 8 positions (or more). We used microfluidics[55] to formulate LNPs with QUANT barcodes[13, 65]. We analyzed the hydrodynamic diameter of each LNP individually using dynamic light scattering and pooled LNPs together if they met 2 inclusion criteria: (i) hydrodynamic diameters between 20 and 200 nm, and (ii) an autocorrelation curve with 1 inflection point (**Fig. 4d, Supplementary Fig. 4b**); We also included a naked DNA barcode, which served as a negative control. We selected these LNP criteria and the control based on experience with a different barcoding system[13]. We studied 2 LNP libraries; as expected, the normalized delivery of the naked DNA barcode was lower than the normalized delivery for barcodes carried by LNPs in library 1 (**Fig. 4e, f**) and library 2 (**Supplementary Fig. 4c, d**). Normalized delivery quantifies how well a LNP performs, relative to all other LNPs in a given sample (**Fig. 4a, Supplementary Fig. 4e**). It is analogous to counts per million in RNA-seq[29], and can describe nanoparticle biodistribution[13, 65].

We intravenously administered the LNPs to WT and Cav1$^{-/-}$ mice at a total DNA dose of 0.5 mg / kg and used FACS to isolate 10 cell types 24 hours after administering the LNPs (**Supplementary Fig. 4f**). We focused on endothelial cells and macrophages since they exist in every tissue; this allowed us to study cell- and tissue-level effects. In LNP library 1, we formulated 128 LNPs; 111 met our 2 inclusion criteria and were pooled together (**Fig. 4c,d, Supplementary Fig. 4g,h**). Multiple lines of evidence suggested Cav1 influenced

nanoparticle delivery in a tissue- and cell-type dependent way. First, the 'total experimental' biodistribution – defined as the total ddPCR counts in the 10 tested cell types – was reduced in Cav1$^{-/-}$ mice, relative to WT mice (**Fig. 5a**). In these pie charts, the area corresponds to total ddPCR counts. It is important to note this pie chart is not equal to the total clearance for the organ, since we did not measure the clearance in every cell type, and the values are not weighted by the percentage of a given cell type within the organ. We chose not to weight the values since the percentage of each cell type within an organ, for all tested organs, was not available.

The decrease in ddPCR counts was not constant across different tissues; Cav1 exerted tissue-specific changes on LNP delivery. For example, the biodistribution to the liver was predominant in WT mice but was much less so in Cav1$^{-/-}$ mice (**Fig. 5a**). The decrease in liver delivery was substantial; the total number of ddPCR counts in the liver of (**Fig. 5b**) Cav1$^{-/-}$ mice decreased by 93%. The Cav1$^{-/-}$ counts in lung and kidney were reduced by 43% and 27%, respectively, relative to WT mice (**Fig. 5c,d**). We then analyzed this effect at the cellular level in all 3 organs. In the liver, most of the decrease in Cav1$^{-/-}$ barcode readouts were due to decreased Kupffer cell delivery (**Fig. 5e**). Delivery to hepatic endothelial cells also decreased, but delivery to hepatocytes was not impacted significantly (**Fig. 5b,e**).

The data above describe the average change in barcode counts for all LNPs. We then quantified how all 111 individual LNPs were affected by Cav1 expression. We multiplied the ddPCR readouts by the normalized delivery, to calculate absolute delivery for each LNP. We then plotted absolute delivery for each LNP in WT and Cav1$^{-/-}$ mice for 3 cell types in the liver (**Fig. 5f**). Delivery to Kupffer cells in Cav1$^{-/-}$ mice was visibly lower than delivery to Kupffer cells in WT mice, even when plotted on a Log_{10} scale (**Fig. 5f**). Delivery to Kupffer cells was affected more than endothelial cells and hepatocytes. Notably, the high throughput analysis of absolute delivery has not been reported before; it is not possible to generate these plots using previous LNP DNA barcoding technologies.

We repeated this experiment using a second LNP library. We rationally designed LNP library 2 to be similar to LNP library 1, with an important distinction: In library 1, LNPs contained the 7C1 lipid, cholesterol, PEG, and the helper lipid 1,2-distearoyl-sn-glycero-3-phosphocholine (DSPC); in library 2, LNPs contained the 7C1 lipid, cholesterol, and PEG. We omitted DSPC to exclude the possibility that the effects we observed in macrophages were due to changes in CD36 expression. CD36 is expressed by macrophages; it acts as a receptor for phosphocholine, which is present in DSPC[68]. Critically, CD36 expression can be modulated by Cav1[69]. We formulated 120 LNPs, of which 115 were stable, pooled, and injected (**Supplementary Fig. 4i-k**). Most of the observations we made with LNP library 1 were consistent in LNP library 2. The 'total experimental' biodistribution was – once again - reduced in Cav1$^{-/-}$ mice, relative to WT mice (**Supplementary Fig. 5a**). There was a pronounced change in delivery to the liver (72% reduction) (**Supplementary Fig. 5b**), and very little change in the kidney (**Supplementary Fig. 5c**). Unlike library 1, in library 2, delivery to the lung was also reduced (**Supplementary Fig. 5d**). When we measured the cell type-specific changes in the liver, we found that Kupffer cell delivery was reduced again, strongly suggesting any effects we observed did not require the phosphocholine group in the

LNPs (**Supplementary Fig. 5b,e**). Delivery to hepatic endothelial cells and hepatocytes were decreased significantly (**Supplementary Fig. 5e**). Finally, we calculated the delivery for all 115 individual LNPs, and were able to visually observe the differences in Kupffer cells more so than hepatic endothelial cells and hepatocytes.

Given the consistent results in Kupffer cells, we investigated whether Cav1 similarly affected pulmonary and renal macrophages (**Fig. 6a**). The total ddPCR counts in pulmonary macrophages did not change with Cav1 expression; renal macrophage delivery decreased, but not significantly. When assessing absolute delivery in WT Kupffer cells as well as pulmonary and renal macrophages, we observed that average nanoparticle delivery was ~10-fold higher in Kupffer cells than in lung and renal macrophages (**Fig. 6b**). To exclude the possibility the Kupffer cell reduction was due to (i) fewer Kupffer cells or (ii) differences in Kupffer cell phenotype in Cav1$^{-/-}$ mice, we measured the (i) number of Kupffer cells / total liver immune cells, and (ii) the expression of CD86 and CD206, 2 markers for Kupffer cell activation in livers of WT and Cav1$^{-/-}$ mice after they were injected with a 1 mg / kg dose of the same previously validated 7C1 LNP we used in our QUANT studies (**Figs. 2,3**). In all previous experiments, we injected 0.5 mg / kg; in this experiment, we injected a 1 mg / kg dose to increase the chance we would observe immune activation. We reasoned this was the most clinically relevant experiment, since all 226 LNPs included the 7C1 compound. The LNPs contained a siRNA that did not target any murine gene (siLuciferase) to minimize the chance gene silencing affected Kupffer cell behavior. We found no differences between number and phenotype of Kupffer cells in WT and Cav1$^{-/-}$ mice (**Fig. 6c-e**). Taken together, these results suggest that caveolin-mediated endocytosis of nanomedicines by macrophages varies with tissue type.

We also observed that Cav1 exerted cell type-specific effects on endothelial cell delivery. We first quantified the ddPCR counts in different endothelial cell beds in WT mice, and found LNPs were delivered to liver, lung, heart, and kidney endothelial cells with differential efficiency (**Supplementary Fig. 6a**). We then calculated the barcode delivery in Cav1$^{-/-}$ mice, and normalized to delivery in WT mice (**Supplementary Fig. 6b**). Cav1$^{-/-}$ had a statistically significant impact on barcode delivery in liver, lung, and heart endothelial cells. Interestingly, delivery to kidney endothelial cells was impacted less. We next measured the individual biodistribution of all 226 LNPs tested in both wild-type and Cav1$^{-/-}$ and found that barcode delivery to endothelial cells was consistently impaired in Cav1$^{-/-}$ mice (**Supplementary Fig. 6c-e**).

Discussion.

Here we show that Cav1 affects LNP delivery in a cell type-specific manner *in vivo*. Delivery to Kupffer cells was significantly altered, leading to changes in nanoparticle biodistribution. Interestingly, Kupffer cell delivery was affected more than delivery to lung or kidney macrophages. These results suggest that Caveolin plays a more prominent role in LNP clearance in Kupffer cells, relative to other macrophage populations. These results are important for drug delivery systems, given that macrophages clear administered LNPs. Given that LNPs are lipid-like nanomaterials with compositions that can be similar to HDL, LDL, and VLDL, it will be interesting to evaluate whether the observations we made here

extend to these 'natural' nanoscale carriers[21, 70]. If so, these results could elucidate how cholesterol is trafficked to different tissues. Our results suggest macrophage uptake changes with tissue type. If future studies elucidate the cell signaling pathways that govern these differences, these cell signaling pathways could be manipulated to alter nanoparticle targeting.

Independent of the Cav1 results, we believe the discovery of QUANT is an important advance. More specifically, we found that a rationally designed ddPCR-based barcode system can quantify delivery with very high sensitivity. Previous DNA barcode technologies designed to track nanoparticle biodistribution could only compare relative biodistribution within the same cell type, but could not be used to compare biodistribution between different cell types[71]. We anticipate future studies further improving the design of QUANT barcodes by incorporating different patterns of chemical modification. Moreover, given that QUANT was able to read out delivery to all tested cell types here, we anticipate it will help scientists identify nanoparticles that target stem cells, immune cells, neurons, and other hard-to-target cell types.

We found that fluorescent biodistribution overestimated delivery to the liver, compared to readouts of the nucleic acid itself. Our results were consistent over several experiments, and echo results generated by scientists studying small molecule delivery[62]. Given that the known mechanisms of nucleic acid degradation[63] are different than the mechanisms that degrade fluorophores, we hypothesize the degradation of the nucleic acid is different from the degradation of the fluorophore. Further studies will be required to confirm or disprove this hypothesis. If confirmed, our results will be important, since most LNPs are thought to preferentially target the liver – often based on fluorescent biodistribution assays. These results could have important implications for nanoparticle discovery pipelines.

It is important note the limitations of our work. First, we only used 1 nucleic acid size; changing the size of QUANT barcodes may better model different classes of nucleic acid drugs. Second, toxic or unstable LNPs will not work with QUANT. Nonetheless, QUANT enables new types of nanoparticle studies that will help elucidate the biological factors that affect LNP targeting and provides proof of principle data that manipulating one gene can be used to retarget nanomedicines.

Materials and Methods

Nanoparticle Formulation.

Nanoparticles were formulated using a microfluidic device as previously described[26]. Briefly, nucleic acids (DNA barcodes) were diluted in 10mM citrate buffer (Teknova) while lipid-amine compounds, alkyl tailed PEG, cholesterol, and helper lipids were diluted in ethanol. All PEGs, cholesterol, and helper lipids were purchased from Avanti Lipids. Citrate and ethanol phases were combined in a microfluidic device by syringes (Hamilton Company) at a flow rate of 600 μL/min and 200 μL/min, respectively.

DNA Barcoding.

Each chemically distinct LNP was formulated to carry its own unique DNA barcode (**Fig. 1a-b**). For example, LNP1 carried DNA barcode 1, while the chemically distinct LNP2 carried DNA barcode 2. 91 nucleotide long single stranded DNA sequences were purchased as ultramers from Integrated DNA Technologies (IDT). Three nucleotides on the 5' and 3' ends were modified with phosphorothioates to reduce exonuclease degradation and improve DNA barcode stability. To ensure equal amplification of each sequence, the we included universal forward and reverse primer regions on all barcodes. Each barcode was distinguished using a unique 8nt sequence. An 8nt sequence can generate over 4^8 (65,536) distinct barcodes. We used 156 distinct 8nt sequences designed by to prevent sequence bleaching on the Illumina MiniSeq™ sequencing machine. A 26nt probe was purchased from IDT with 5' FAM as the fluorophore, while internal Zen and 3' Iowa Black FQ were used as quenchers. Fluorescent barcode was purchased from IDT with AlexaFluor647 or AlexaFluor488 conjugated to the 5' end.

In Vitro L2K.

Immortalized Mouse Aortic Endothelial Cells (IMAECs) were seeded at 10,000 cells per well in a 96-well plate. 24 hours after seeding, QUANT barcodes or Alexa-647-barcodes were transfected using Lipofectamine 2000. 24 hours after transfection, DNA was isolated from cells treated with QUANT barcodes and fluorescent barcodes were measured using a DN Accuri C6 flow cytometer.

Nanoparticle Characterization.

LNP hydrodynamic diameter was measured using high throughput dynamic light scattering (DLS) (DynaPro Plate Reader II, Wyatt). LNPs were diluted in sterile 1X PBS to a concentration of ~0.06 μg/mL, and analyzed. To avoid using unstable LNPs, and to enable sterile purification using a 0.22 μm filter, LNPs were included only if they met the criteria of monodisperse population with diameter between 20 and 200nm. Particles that met these criteria were dialyzed with 1X phosphate buffered saline (PBS, Invitrogen), and were sterile filtered with a 0.22 μm filter.

Animal Experiments.

All animal experiments were performed in accordance with the Georgia Institute of Technology IACUC. C57BL/6J (#000664) and Caveolin1$^{-/-}$ (#007083) mice were purchased from The Jackson Laboratory and used between 5–8 weeks of age. In all *in vitro* and *in* vivo experiments, we used N=3–5 group. Mice were injected intravenously via the lateral tail vein. The nanoparticle concentration was determined using NanoDrop (Thermo Scientific). For *in vivo* nanoparticle screens, mice were administered at a dose of 0.5 mg/kg.

Cell Isolation & Staining.

Cells were isolated 24 (for screens) or 96 (for *in vivo* gene editing) hours after injection with LNPs unless otherwise noted. Mice were perfused with 20 mL of 1X PBS through the right atrium. Tissues were finely cut, and then placed in a digestive enzyme solution with Collagenase Type I (Sigma Aldrich), Collagenase XI (Sigma Aldrich) and Hyaluronidase

(Sigma Aldrich) at 37 ºC at 550 rpm for 45 minutes. The digestive enzyme for heart and spleen included Collagenase IV[7, 56, 58]. Cell suspension was filtered through 70μm mesh and red blood cells were lysed. Cells were stained to identify specific cell populations and sorted using the BD FacsFusion and BD Facs Aria IIIu cell sorters in the Georgia Institute of Technology Cellular Analysis Core. For *in vitro* flow cytometry experiments, a BD Accuri C6 was used in the Georgia Institute of Technology Cellular Analysis Core. The antibody clones used were: anti-CD31 (390, BioLegend), anti-CD45.2 (104, BioLegend), anti-CD68 (FA-11, Biolegend), and anti-CD11b (M1/70, Biolegend). Representative flow gates are located in **Supplementary Figure 1**.

ddPCR.

The QX200™ Droplet Digital™ PCR System (Bio-Rad) was used to prep and analyze all ddPCR results. All PCR samples were prepared with 10μL ddPCR with ddPCR™ Supermix for Probes (BioRad), 1μL of primer and probe mix (solution of 10μM of target probe and 20μM of Reverse/Forward Primers), 1μL of template/TE buffer, and 8μL water. 20μL of each reaction and 70μL of Droplet Generation Oil for Probes (Bio-Rad) were loaded into DG8™ Cartridges and covered with DG8™ Gaskets. Cartridges were placed in the QX200™ Droplet Generator to create water-oil emulsion droplets. Cycle conditions for PCR were as follows: 1 cycle of 95º for 10 minutes, followed by 40 cycles of 94ºC for 30 seconds, 60ºC for 1 minute, and 1 cycle of 95ºC for 10 minutes. Plates were stored at 4ºC until ran on the QX200™ Droplet Digital™ PCR System. For each biological rep, 3 technical repetitions were completed. In all cases, technical reps were averaged. Technical reps were only excluded if they saturated the detection or showed inconsistent positive event amplitudes.

PCR Amplification for Illumina Sequencing.

All samples were amplified and prepared for sequencing using a two-step, nested PCR protocol **(Supplementary Figure 1e)**. More specifically, 2 μL of primers (10 uM for Base Reverse/Forward) were added to 5 μL of Kapa HiFi 2X master mix, and 3 μL template DNA/water. This first PCR reaction was ran for 20–30 cycles. The second PCR, to add Nextera XT chemistry, indices, and i5/i7 adapter regions was ran for 5–10 cycles and used the product from ‘PCR 1’ as template. Dual-indexed samples were ran on a 2% agarose gel to ensure that PCR reaction occurred before being pooled and purified using BluePippin (Sage Science).

Deep Sequencing.

Illumina sequencing was conducted in Georgia Institute of Technology’s Molecular Evolution core. Runs were performed on an Illumina Miniseq. Primers were designed based on Nextera XT adapter sequences.

Barcode Sequencing Normalization.

Counts for each particle, per cell type, were normalized to the barcoded LNP mixture applied to cells or injected into the mouse.

Endothelial RNA interference.

C57BL/6J and Caveolin1$^{-/-}$ mice were injected with 7C1 carrying 1 mg/kg siCTRL (siLuc) (AxoLabs). In all cases, siRNAs were chemically modified at the 2' position to increase stability and negate immunostimulation. 72 hours after injection, tissues were isolated and protein expression was determined via flow cytometry. ICAM2 MFI in siLuc-treated mice (for each background) was normalized to 100 percent.

Data Analysis & Statistics.

Sequencing results were processed using a custom R script to extract raw barcode counts for each tissue. These raw counts were then normalized with an R script prior for further analysis. Statistical analysis was done using GraphPad Prism 7; more specifically, 1-tail T-test, Paired 2tail T-test, or One-way ANOVAs were used where appropriate. Data is plotted as mean ± standard error mean unless otherwise stated.

Data Access.

The data, analyses, and scripts used to generate all figures in the paper are available upon request to james.dahlman@bme.gatech.edu.

Supplementary Material

Refer to Web version on PubMed Central for supplementary material.

Acknowledgments.

The authors thank Sommer Durham and the Georgia Tech Cellular Analysis and Cytometry Core. Additionally, the authors thank Dalia Arafat and the Genome Analysis Core. The authors thank Marielena Gamboa Castro for helpful discussion. J.E.D. thanks Jordan Cattie and Taylor E. Shaw.

Funding. C.D.S., M.L., and J.E.D. were funded by Georgia Tech startup funds (awarded to J.E.D.). C.D.S. was funded by the NIH-sponsored Research Training Program in Immunoengineering (T32EB021962). This content is solely the responsibility of the authors and does not necessarily represent the official views of the National Institutes of Health. Research was funded by the Cystic Fibrosis Research Foundation (DAHLMA15XX0, awarded to J.E.D.), the Parkinson's Disease Foundation (PDF-JFA-1860, awarded to J.E.D.), and the Bayer Hemophilia Awards Program (AGE DTD, awarded to J.E.D.).

Citations

1. Pasi KJ; Rangarajan S; Georgiev P; Mant T; Creagh MD; Lissitchkov T; Bevan D; Austin S; Hay CR; Hegemann I; Kazmi R; Chowdary P; Gercheva-Kyuchukova L; Mamonov V; Timofeeva M; Soh CH; Garg P; Vaishnaw A; Akinc A; Sorensen B; Ragni MV N Engl J Med 2017, 377, (9), 819–828. [PubMed: 28691885]
2. Adams D; Gonzalez-Duarte A; O'Riordan WD; Yang CC; Ueda M; Kristen AV; Tournev I; Schmidt HH; Coelho T; Berk JL; Lin KP; Vita G; Attarian S; Plante-Bordeneuve V; Mezei MM; Campistol JM; Buades J; Brannagan TH 3rd; Kim BJ; Oh J; Parman Y; Sekijima Y; Hawkins PN; Solomon SD; Polydefkis M; Dyck PJ; Gandhi PJ; Goyal S; Chen J; Strahs AL; Nochur SV; Sweetser MT; Garg PP; Vaishnaw AK; Gollob JA; Suhr OB N Engl J Med 2018, 379, (1), 11–21. [PubMed: 29972753]
3. Coelho T; Adams D; Silva A; Lozeron P; Hawkins PN; Mant T; Perez J; Chiesa J; Warrington S; Tranter E; Munisamy M; Falzone R; Harrop J; Cehelsky J; Bettencourt BR; Geissler M; Butler JS; Sehgal A; Meyers RE; Chen Q; Borland T; Hutabarat RM; Clausen VA; Alvarez R; Fitzgerald K; Gamba-Vitalo C; Nochur SV; Vaishnaw AK; Sah DW; Gollob JA; Suhr OB N Engl J Med 2013, 369, (9), 819–29. [PubMed: 23984729]

4. Lorenzer C; Dirin M; Winkler AM; Baumann V; Winkler J J Control Release 2015, 203, 1–15. [PubMed: 25660205]
5. Tsoi KM; MacParland SA; Ma XZ; Spetzler VN; Echeverri J; Ouyang B; Fadel SM; Sykes EA; Goldaracena N; Kaths JM; Conneely JB; Alman BA; Selzner M; Ostrowski MA; Adeyi OA; Zilman A; McGilvray ID; Chan WC Nat Mater 2016, 15, (11), 1212–1221. [PubMed: 27525571]
6. Zhang YN; Poon W; Tavares AJ; McGilvray ID; Chan WCW J Control Release 2016, 240, 332–348. [PubMed: 26774224]
7. Dahlman JE; Barnes C; Khan OF; Thiriot A; Jhunjunwala S; Shaw TE; Xing Y; Sager HB; Sahay G; Speciner L; Bader A; Bogorad RL; Yin H; Racie T; Dong Y; Jiang S; Seedorf D; Dave A; Singh Sandhu K; Webber MJ; Novobrantseva T; Ruda VM; LyttonJeanAbigail KR; Levins CG; Kalish B; Mudge DK; Perez M; Abezgauz L; Dutta P; Smith L; Charisse K; Kieran MW; Fitzgerald K; Nahrendorf M; Danino D; Tuder RM; von Andrian UH; Akinc A; Panigrahy D; Schroeder A; Koteliansky V; Langer R; Anderson DG Nat Nano 2014, 9, (8), 648–655.
8. Hao J; Kos P; Zhou K; Miller JB; Xue L; Yan Y; Xiong H; Elkassih S; Siegwart DJ J Am Chem Soc 2015, 29, (1520–5126 (Electronic)), 9206–9209.
9. Dong Y; Love KT; Dorkin JR; Sirirungruang S; Zhang Y; Chen D; Bogorad RL; Yin H; Chen Y; Vegas AJ; Alabi CA; Sahay G; Olejnik KT; Wang W; Schroeder A; Lytton-Jean AK; Siegwart DJ; Akinc A; Barnes C; Barros SA; Carioto M; Fitzgerald K; Hettinger J; Kumar V; Novobrantseva TI; Qin J; Querbes W; Koteliansky V; Langer R; Anderson DG Proceedings of the National Academy of Sciences of the United States of America 2014, 111, (11), 395560.
10. Siegwart DJ; Whitehead KA; Nuhn L; Sahay G; Cheng H; Jiang S; Ma M; Lytton-Jean A; Vegas A; Fenton P; Levins CG; Love KT; Lee H; Cortez C; Collins SP; Li YF; Jang J; Querbes W; Zurenko C; Novobrantseva T; Langer R; Anderson DG Proceedings of the National Academy of Sciences of the United States of America 2011, 108, (32), 12996–3001. [PubMed: 21784981]
11. Love KT; Mahon KP; Levins CG; Whitehead KA; Querbes W; Dorkin JR; Qin J; Cantley W; Qin LL; Racie T; Frank-Kamenetsky M; Yip KN; Alvarez R; Sah DW; de Fougerolles A; Fitzgerald K; Koteliansky V; Akinc A; Langer R; Anderson DG Proceedings of the National Academy of Sciences of the United States of America 2010, 107, (5), 1864–9. [PubMed: 20080679]
12. Akinc A; Zumbuehl A; Goldberg M; Leshchiner ES; Busini V; Hossain N; Bacallado SA; Nguyen DN; Fuller J; Alvarez R; Borodovsky A; Borland T; Constien R; de Fougerolles A; Dorkin JR; Narayanannair Jayaprakash K; Jayaraman M; John M; Koteliansky V; Manoharan M; Nechev L; Qin J; Racie T; Raitcheva D; Rajeev KG; Sah DW; Soutschek J; Toudjarska I; Vornlocher HP; Zimmermann TS; Langer R; Anderson DG Nat Biotechnol 2008, 26, (5), 561–9. [PubMed: 18438401]
13. Paunovska K; Sago CD; Monaco CM; Hudson WH; Castro MG; Rudoltz TG; Kalathoor S; Vanover DA; Santangelo PJ; Ahmed R; Bryksin AV; Dahlman JE Nano Lett 2018, 18, (3), 2148–2157. [PubMed: 29489381]
14. Patel S; Ashwanikumar N; Robinson E; DuRoss A; Sun C; Murphy-Benenato KE; Mihai C; Almarsson O; Sahay G Nano Lett 2017, 17, (9), 5711–5718. [PubMed: 28836442]
15. Sahay G; Querbes W; Alabi C; Eltoukhy A; Sarkar S; Zurenko C; Karagiannis E; Love K; Chen D; Zoncu R; Buganim Y; Schroeder A; Langer R; Anderson DG Nat Biotechnol 2013, 31, (7), 653–8. [PubMed: 23792629]
16. Gilleron J; Querbes W; Zeigerer A; Borodovsky A; Marsico G; Schubert U; Manygoats K; Seifert S; Andree C; Stoter M; Epstein-Barash H; Zhang L; Koteliansky V; Fitzgerald K; Fava E; Bickle M; Kalaidzidis Y; Akinc A; Maier M; Zerial M Nat Biotechnol 2013, 31, (7), 638–46. [PubMed: 23792630]
17. Wittrup A; Ai A; Liu X; Hamar P; Trifonova R; Charisse K; Manoharan M; Kirchhausen T; Lieberman J Nat Biotechnol 2015, 33, (8), 870–6. [PubMed: 26192320]
18. Bertrand N; Grenier P; Mahmoudi M; Lima EM; Appel EA; Dormont F; Lim JM; Karnik R; Langer R; Farokhzad OC Nature communications 2017, 8, (1), 777.
19. Akinc A; Querbes W; De S; Qin J; Frank-Kamenetsky M; Jayaprakash KN; Jayaraman M; Rajeev KG; Cantley WL; Dorkin JR; Butler JS; Qin L; Racie T; Sprague A; Fava E; Zeigerer A; Hope MJ; Zerial M; Sah DW; Fitzgerald K; Tracy MA; Manoharan M; Koteliansky V; Fougerolles A; Maier MA Mol Ther 2010, 18, (7), 1357–64. [PubMed: 20461061]

20. Willoughby JLS; Chan A; Sehgal A; Butler JS; Nair JK; Racie T; Shulga-Morskaya S; Nguyen T; Qian K; Yucius K; Charisse K; van Berkel TJC; Manoharan M; Rajeev KG; Maier MA; Jadhav V; Zimmermann TS Mol Ther 2018, 26, (1), 105–114. [PubMed: 28988716]
21. Paunovska K; Gil CJ; Lokugamage MP; Sago CD; Sato M; Lando GN; Gamboa Castro M; Bryksin AV; Dahlman JE ACS nano 2018, 12, (8), 8341–8349. [PubMed: 30016076]
22. Wang M; Thanou M Pharmacological research 2010, 62, (2), 90–9. [PubMed: 20380880]
23. Ostergaard ME; Yu J; Kinberger GA; Wan WB; Migawa MT; Vasquez G; Schmidt K; Gaus HJ; Murray HM; Low A; Swayze EE; Prakash TP; Seth PP Bioconjug Chem 2015, 26, (8), 1451–5. [PubMed: 26011654]
24. El-Sayed IH; Huang X; El-Sayed MA Cancer letters 2006, 239, (1), 129–35. [PubMed: 16198049]
25. Stevens PJ; Sekido M; Lee RJ Pharmaceutical research 2004, 21, (12), 2153–7. [PubMed: 15648245]
26. Davis ME; Zuckerman JE; Choi CH; Seligson D; Tolcher A; Alabi CA; Yen Y; Heidel JD; Ribas A Nature 2010, 464, (7291), 1067–70. [PubMed: 20305636]
27. Kheirolomoom A; Kim CW; Seo JW; Kumar S; Son DJ; Gagnon MK; Ingham ES; Ferrara KW; Jo H ACS nano 2015, 9, (9), 8885–97. [PubMed: 26308181]
28. Muro S; Garnacho C; Champion JA; Leferovich J; Gajewski C; Schuchman EH; Mitragotri S; Muzykantov VR Mol Ther 2008, 16, (8), 1450–8. [PubMed: 18560419]
29. Conesa A; Madrigal P; Tarazona S; Gomez-Cabrero D; Cervera A; McPherson A; Szczesniak MW; Gaffney DJ; Elo LL; Zhang X; Mortazavi A Genome biology 2016, 17, 13. [PubMed: 26813401]
30. Lee MN; Ye C; Villani AC; Raj T; Li W; Eisenhaure TM; Imboywa SH; Chipendo PI; Ran FA; Slowikowski K; Ward LD; Raddassi K; McCabe C; Lee MH; Frohlich IY; Hafler DA; Kellis M; Raychaudhuri S; Zhang F; Stranger BE; Benoist CO; De Jager PL; Regev A; Hacohen N Science 2014, 343, (6175), 1246980. [PubMed: 24604203]
31. Vanlandewijck M; He L; Mae MA; Andrae J; Ando K; Del Gaudio F; Nahar K; Lebouvier T; Lavina B; Gouveia L; Sun Y; Raschperger E; Rasanen M; Zarb Y; Mochizuki N; Keller A; Lendahl U; Betsholtz C Nature 2018, 554, (7693), 475–480. [PubMed: 29443965]
32. Zeisel A; Munoz-Manchado AB; Codeluppi S; Lonnerberg P; La Manno G; Jureus A; Marques S; Munguba H; He L; Betsholtz C; Rolny C; Castelo-Branco G; Hjerling-Leffler J; Linnarsson S Science 2015, 347, (6226), 1138–42. [PubMed: 25700174]
33. Rozenblatt-Rosen O; Stubbington MJT; Regev A; Teichmann SA Nature 2017, 550, (7677), 451–453. [PubMed: 29072289]
34. Collinet C; Stoter M; Bradshaw CR; Samusik N; Rink JC; Kenski D; Habermann B; Buchholz F; Henschel R; Mueller MS; Nagel WE; Fava E; Kalaidzidis Y; Zerial M Nature 2010, 464, (7286), 243–9. [PubMed: 20190736]
35. Sigismund S; Confalonieri S; Ciliberto A; Polo S; Scita G; Di Fiore PP Physiological reviews 2012, 92, (1), 273–366. [PubMed: 22298658]
36. Palm W; Thompson CB Nature 2017, 546, (7657), 234–242. [PubMed: 28593971]
37. Doherty GJ; McMahon HT Annu Rev Biochem 2009, 78, 857–902. [PubMed: 19317650]
38. Voigt J; Christensen J; Shastri VP Proceedings of the National Academy of Sciences of the United States of America 2014, 111, (8), 2942–7. [PubMed: 24516167]
39. Shamay Y; Shah J; Isik M; Mizrachi A; Leibold J; Tschaharganeh DF; Roxbury D; Budhathoki-Uprety J; Nawaly K; Sugarman JL; Baut E; Neiman MR; Dacek M; Ganesh KS; Johnson DC; Sridharan R; Chu KL; Rajasekhar VK; Lowe SW; Chodera JD; Heller DA Nat Mater 2018, 17, (4), 361–368. [PubMed: 29403054]
40. Cheng Z; Liu L; Wang Z; Cai Y; Xu Q; Chen P International journal of molecular sciences 2018, 19, (2).
41. Shihata WA; Putra MRA; Chin-Dusting JPF. Frontiers in pharmacology 2017, 8, 567. [PubMed: 28970796]
42. Gvaramia D; Blaauboer ME; Hanemaaijer R; Everts V Matrix biology : journal of the International Society for Matrix Biology 2013, 32, (6), 307–15. [PubMed: 23583521]
43. Yokomori H; Ando W; Yoshimura K; Yamazaki H; Takahashi Y; Oda M Micron (Oxford, England : 1993) 2015, 76, 52–61.

44. Maniatis NA; Chernaya O; Shinin V; Minshall RD Advances in experimental medicine and biology 2012, 729, 157–79. [PubMed: 22411320]
45. Sotgia F; Martinez-Outschoorn UE; Pavlides S; Howell A; Pestell RG; Lisanti MP Breast cancer research : BCR 2011, 13, (4), 213. [PubMed: 21867571]
46. Witkiewicz AK; Dasgupta A; Sotgia F; Mercier I; Pestell RG; Sabel M; Kleer CG; Brody JR; Lisanti MP Am J Pathol 2009, 174, (6), 2023–34. [PubMed: 19411448]
47. Yang G; Truong LD; Wheeler TM; Thompson TC Cancer Res 1999, 59, (22), 5719–23. [PubMed: 10582690]
48. Wiechen K; Sers C; Agoulnik A; Arlt K; Dietel M; Schlag PM; Schneider U Am J Pathol 2001, 158, (3), 833–9. [PubMed: 11238032]
49. Gaudreault SB; Dea D; Poirier J Neurobiology of aging 2004, 25, (6), 753–9. [PubMed: 15165700]
50. Kassan A; Egawa J; Zhang Z; Almenar-Queralt A; Nguyen QM; Lajevardi Y; Kim K; Posadas E; Jeste DV; Roth DM; Patel PM; Patel HH; Head BP Journal of neurophysiology 2017, 117, (1), 436–444. [PubMed: 27832597]
51. Chand S; Edwards NC; Chue CD; Jesky M; Stringer S; Simmonds MJ; Duff CE; Cockwell P; Harper L; Steeds RP; Townend JN; Ferro CJ; Borrows R Nephrology, dialysis, transplantation : official publication of the European Dialysis and Transplant Association - European Renal Association 2016, 31, (7), 1140–4.
52. Tourkina E; Bonner M; Oates J; Hofbauer A; Richard M; Znoyko S; Visconti RP; Zhang J; Hatfield CM; Silver RM; Hoffman S Fibrogenesis & tissue repair 2011, 4, (1), 15.
53. Del Galdo F; Lisanti MP; Jimenez SA Current opinion in rheumatology 2008, 20, (6), 713–9. [PubMed: 18949888]
54. Zhang Y; Sloan SA; Clarke LE; Caneda C; Plaza CA; Blumenthal PD; Vogel H; Steinberg GK; Edwards MS; Li G; Duncan JA 3rd; Cheshier SH; Shuer LM; Chang EF; Grant GA; Gephart MG; Barres BA Neuron 2016, 89, (1), 37–53. [PubMed: 26687838]
55. Chen D; Love KT; Chen Y; Eltoukhy AA; Kastrup C; Sahay G; Jeon A; Dong Y; Whitehead KA; Anderson DG J Am Chem Soc 2012, 134, (16), 6948–51. [PubMed: 22475086]
56. Sager HB; Dutta P; Dahlman JE; Hulsmans M; Courties G; Sun Y; Heidt T; Vinegoni C; Borodovsky A; Fitzgerald K; Wojtkiewicz GR; Iwamoto Y; Tricot B; Khan OF; Kauffman KJ; Xing Y; Shaw TE; Libby P; Langer R; Weissleder R; Swirski FK; Anderson DG; Nahrendorf M Science translational medicine 2016, 8, (342), 342ra80–342ra80.
57. Yun S; Budatha M; Dahlman JE; Coon BG; Cameron RT; Langer R; Anderson DG; Baillie G; Schwartz MA Nat Cell Biol 2016.
58. Sager HB; Hulsmans M; Lavine KJ; Moreira MB; Heidt T; Courties G; Sun Y; Iwamoto Y; Tricot B; Khan OF; Dahlman JE; Borodovsky A; Fitzgerald K; Anderson DG; Weissleder R; Libby P; Swirski FK; Nahrendorf M Circ Res 2016, 119, (7), 853–64. [PubMed: 27444755]
59. White K; Lu Y; Annis S; Hale AE; Chau BN; Dahlman JE; Hemann C; Opotowsky AR; Vargas SO; Rosas I; Perrella MA; Osorio JC; Haley KJ; Graham BB; Kumar R; Saggar R; Saggar R; Wallace WD; Ross DJ; Khan OF; Bader A; Gochuico BR; Matar M; Polach K; Johannessen NM; Prosser HM; Anderson DG; Langer R; Zweier JL; Bindoff LA; Systrom D; Waxman AB; Jin RC; Chan SY EMBO Mol Med 2015, 7, (6), 695–713. [PubMed: 25825391]
60. Platt RJ; Chen S; Zhou Y; Yim MJ; Swiech L; Kempton HR; Dahlman JE; Parnas O; Eisenhaure TM; Jovanovic M; Graham DB; Jhunjhunwala S; Heidenreich M; Xavier RJ; Langer R; Anderson DG; Hacohen N; Regev A; Feng G; Sharp PA; Zhang F Cell 2014, 159, (2), 440–55. [PubMed: 25263330]
61. Sahay G; Alakhova DY; Kabanov AV J Control Release 2010, 145, (3), 182–95. [PubMed: 20226220]
62. Meng F; Wang J; Ping Q; Yeo Y ACS nano 2018, 12, (7), 6458–6468. [PubMed: 29920064]
63. Yang W Quarterly reviews of biophysics 2011, 44, (1), 1-93.
64. Hindson CM; Chevillet JR; Briggs HA; Gallichotte EN; Ruf IK; Hindson BJ; Vessella RL; Tewari M Nat Methods 2013, 10, (10), 1003–5. [PubMed: 23995387]
65. Dahlman JE; Kauffman KJ; Xing Y; Shaw TE; Mir FF; Dlott CC; Langer R; Anderson DG; Wang ET Proceedings of the National Academy of Sciences of the United States of America 2017, 114, (8), 2060–2065. [PubMed: 28167778]

66. Ni CW; Kumar S; Ankeny CJ; Jo H Vascular cell 2014, 6, (1), 7.
67. Yaari Z; da Silva D; Zinger A; Goldman E; Kajal A; Tshuva R; Barak E; Dahan N; Hershkovitz D; Goldfeder M; Roitman JS; Schroeder A Nature communications 2016, 7, 13325.
68. Podrez EA; Poliakov E; Shen Z; Zhang R; Deng Y; Sun M; Finton PJ; Shan L; Gugiu B; Fox PL; Hoff HF; Salomon RG; Hazen SL J Biol Chem 2002, 277, (41), 38503–16. [PubMed: 12105195]
69. Mattern HM; Raikar LS; Hardin CD International journal of physiology, pathophysiology and pharmacology 2009, 1, (1), 1–14.
70. Kuai R; Li D; Chen YE; Moon JJ; Schwendeman A ACS nano 2016, 10, (3), 3015–3041. [PubMed: 26889958]
71. Lokugamage MP; Sago CD; Dahlman JE Current Opinion in Biomedical Engineering 2018, 7, 1–8. [PubMed: 30931416]

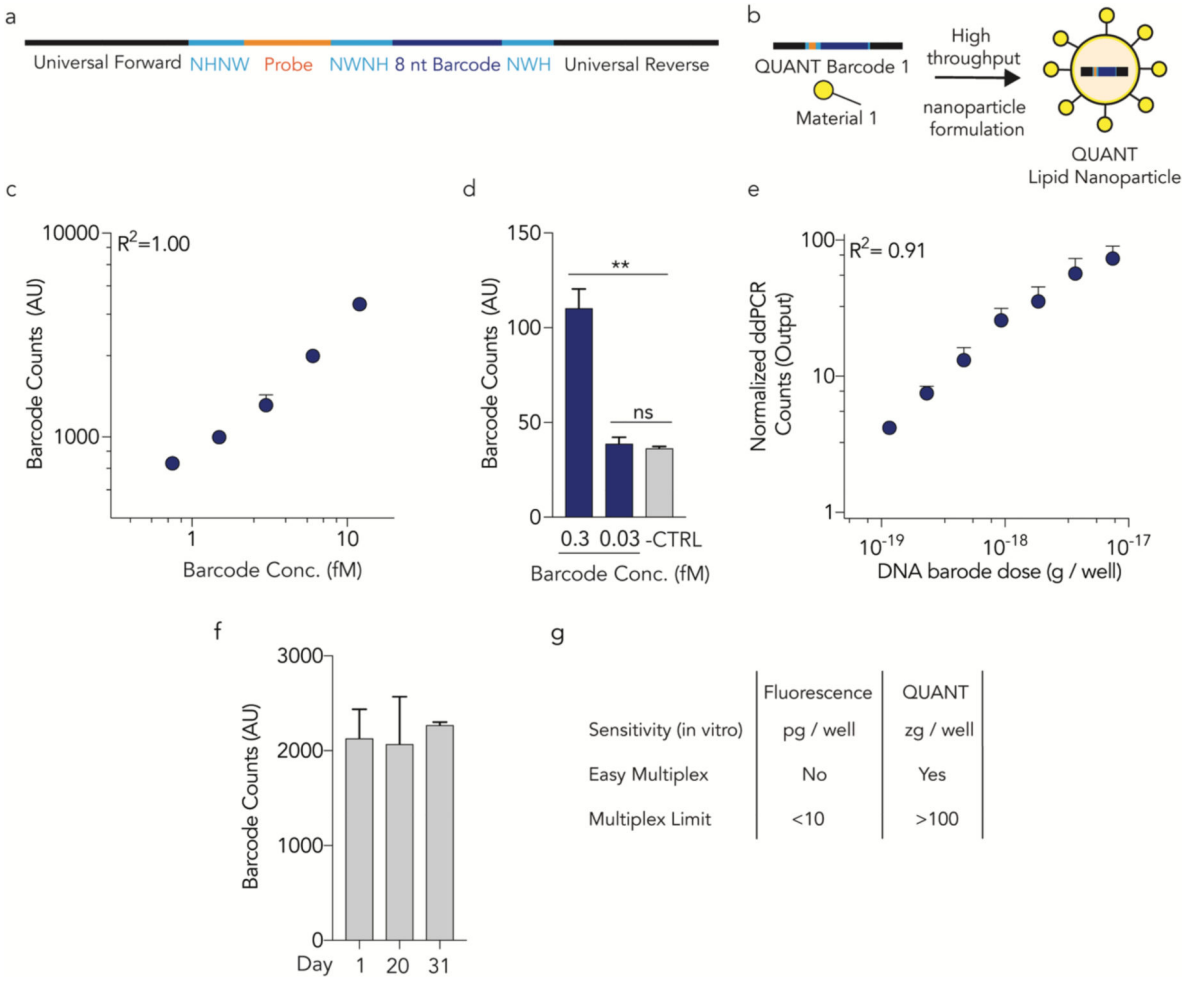

Figure 1.

QUANT barcodes are rationally designed to provide highly sensitive readouts of nanoparticle delivery. **(a)** QUANT barcodes contain universal primer sites, an 8 nucleotide barcode region, a probe binding site, and split semi-randomized regions. These designs reduce DNA secondary structure and increase DNA polymerase access. **(b)** Barcodes can be formulated into chemically distinct lipid nanoparticles using high throughput microfluidics. **(c)** Standard curve of QUANT barcodes diluted in TE buffer; **(d)** barcodes can be identified above background at 300 aM concentrations. **p<0.01, 2 tailed ttest. **(e)** An *in vitro* standard curve; barcodes were quantified 24 hours after being delivered to cell using Lipofectamine 2000. **(f)** QUANT barcode readouts immediately after DNA was isolated from cells following *in vivo* nanoparticle delivery, or after the samples were stored at −20˚C for 20 or 31 days. Each experiment was performed using different stock reagents, demonstrating the repeatability of the assay. **(g)** Comparison of fluorescence and QUANT-based methods of analyzing nanoparticle biodistribution.

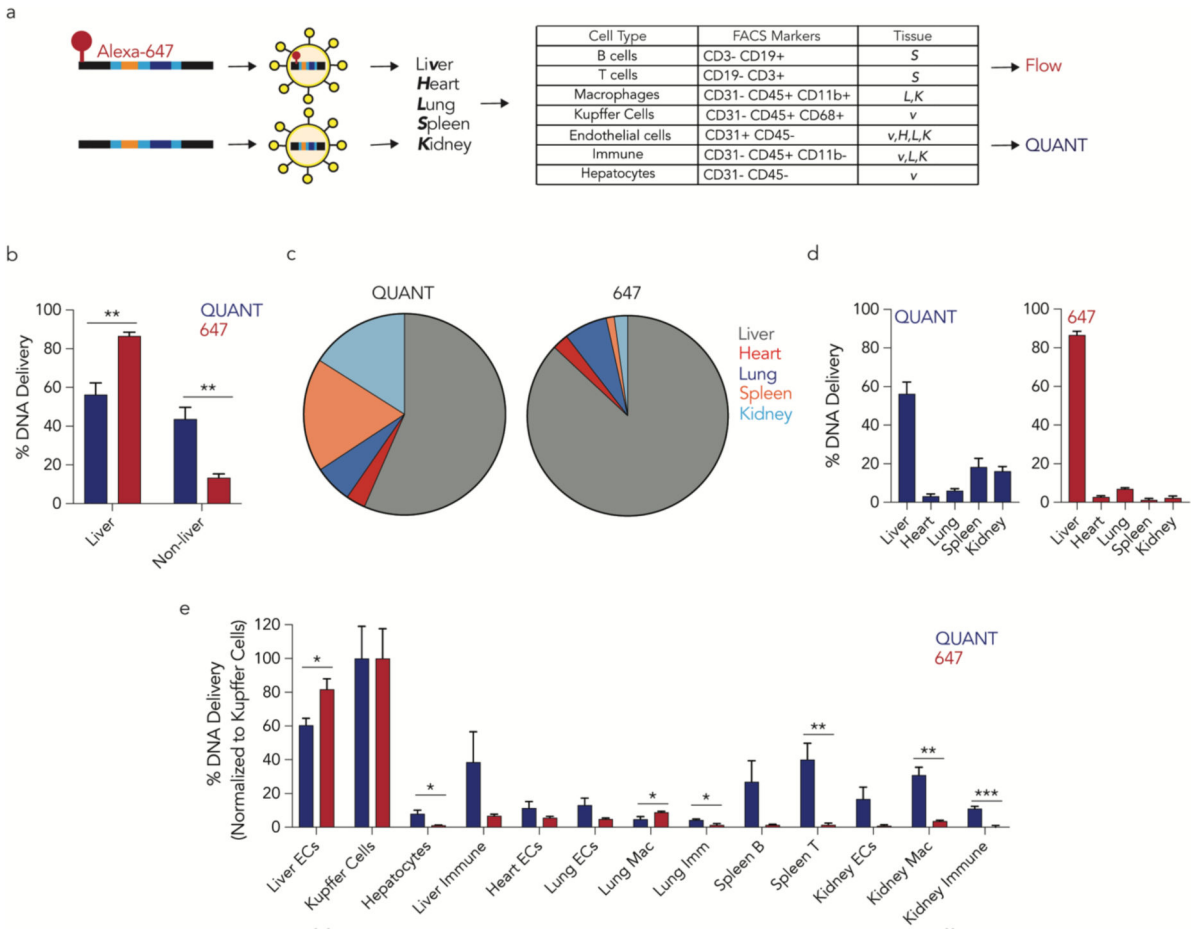

Figure 2.

A direct comparison of fluorescent- and ddPCR-based biodistribution *in vivo* reveals differences. **(a)** QUANT barcodes with (or without) a fluorophore were formulated into a LNP and injected intravenously. Five tissues were isolated and barcode delivery to 13 cell types isolated by FACS was measured by QUANT or fluorescence. **(b)** Cumulative biodistribution measured by QUANT or fluorescence in liver and non-liver cell types. **p<0.01, 2 tailed t-test. **(c,d)** Cumulative biodistribution within the 5 tissues examined by QUANT and fluorescence. Fluorescence readouts overestimate liver delivery. **(e)** Comparison of biodistribution in the 13 cell types examined by QUANT and fluorescence. *p<0.05, **p<0.01, ***p<0.001, 2 tailed t-test. ECs; endothelial cells. Mac; macrophage. Imm; immune.

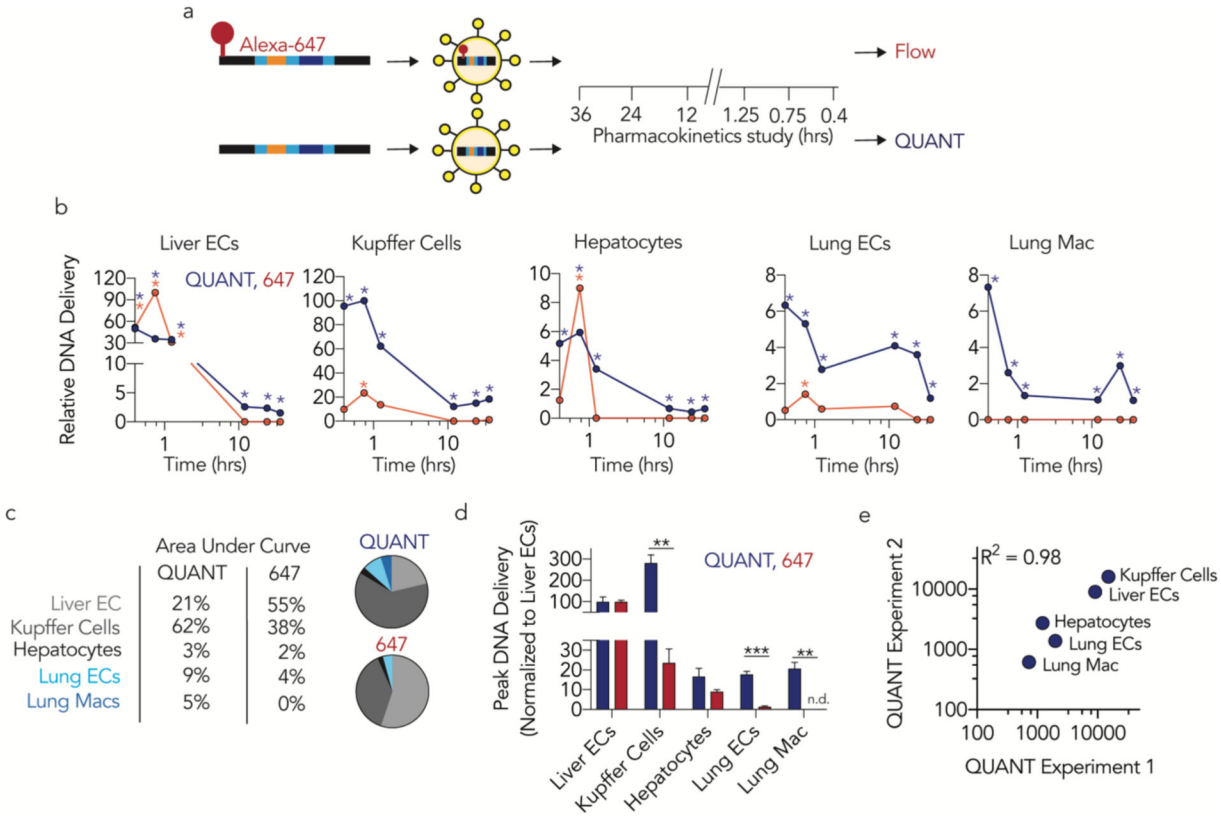

Figure 3.

QUANT biodistribution is more sensitive than fluorescence *in vivo*. **(a)** QUANT barcodes with (or without) a fluorophore were formulated into LNPs, injected intravenously, and isolated at different timepoints. Nanoparticle distribution was measured using QUANT or fluorescence. **(b)** Relative nanoparticle biodistribution (normalized to maximal signal in any cell type) 0.4, 0.75, 1.25, 12, 24, and 36 hours after administration of a LNP carrying 647-QUANT barcode or QUANT barcodes at a dose of 0.5 mg / kg. Asterisk denotes a signal that was significantly different than PBS-treated mice. **(c)** Comparisons of area under the curve as measured by QUANT or fluorescence. Delivery to the lungs was underestimated by >3 fold by fluorescence. **(d)** Peak DNA delivery (normalized to liver ECs) as measured by QUANT and fluorescence. No fluorescent signal was detected in lung macrophages. **p<0.01, ***p<0.001 2 tailed t-test. **(e)** R^2 analysis of QUANT absolutely counts from the 1 hour timepoint (Figure 2) and the 1.25 hour timepoint (Figure 3) across two experiments performed on separate days.

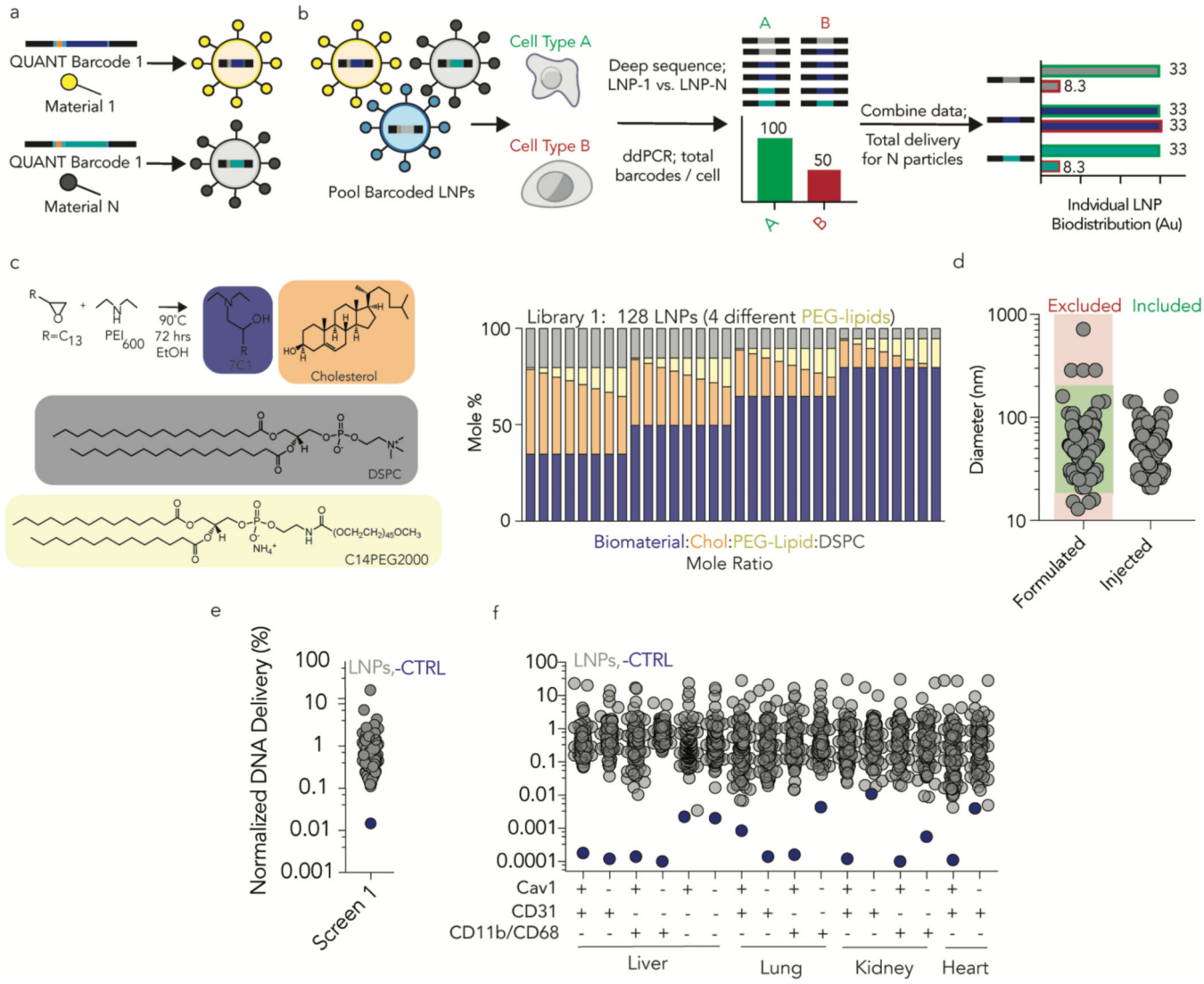

Figure 4.

QUANT quantifies how over 100 LNPs deliver nucleic acids in wild-type and Cav1$^{-/-}$ mice. **(a)** Unique QUANT barcodes can be formulated into chemically distinct nanoparticles. **(b)** QUANT ddPCR readouts can be coupled with deep sequencing to measure absolute delivery mediated by >100 LNPs at once *in vivo*. **(c)** LNP library 1 was synthesized with the amine 7C1, Cholesterol, DSPC, and PEG compounds at variable molar ratios; 128 different LNPs were formulated for screen 1. **(d)** The diameter of each LNP in screen 1 was measured individually; stable LNPs, with diameters between 20 and 200 nm were included. **(e)** The average normalized delivery from all LNPs and the naked barcode (negative control) from screen 1. **(f)** As expected, the naked barcode – which was the negative control – was delivered less efficiently than barcodes carried by LNPs in every cell type, both in WT mice and Cav1$^{-/-}$ mice.

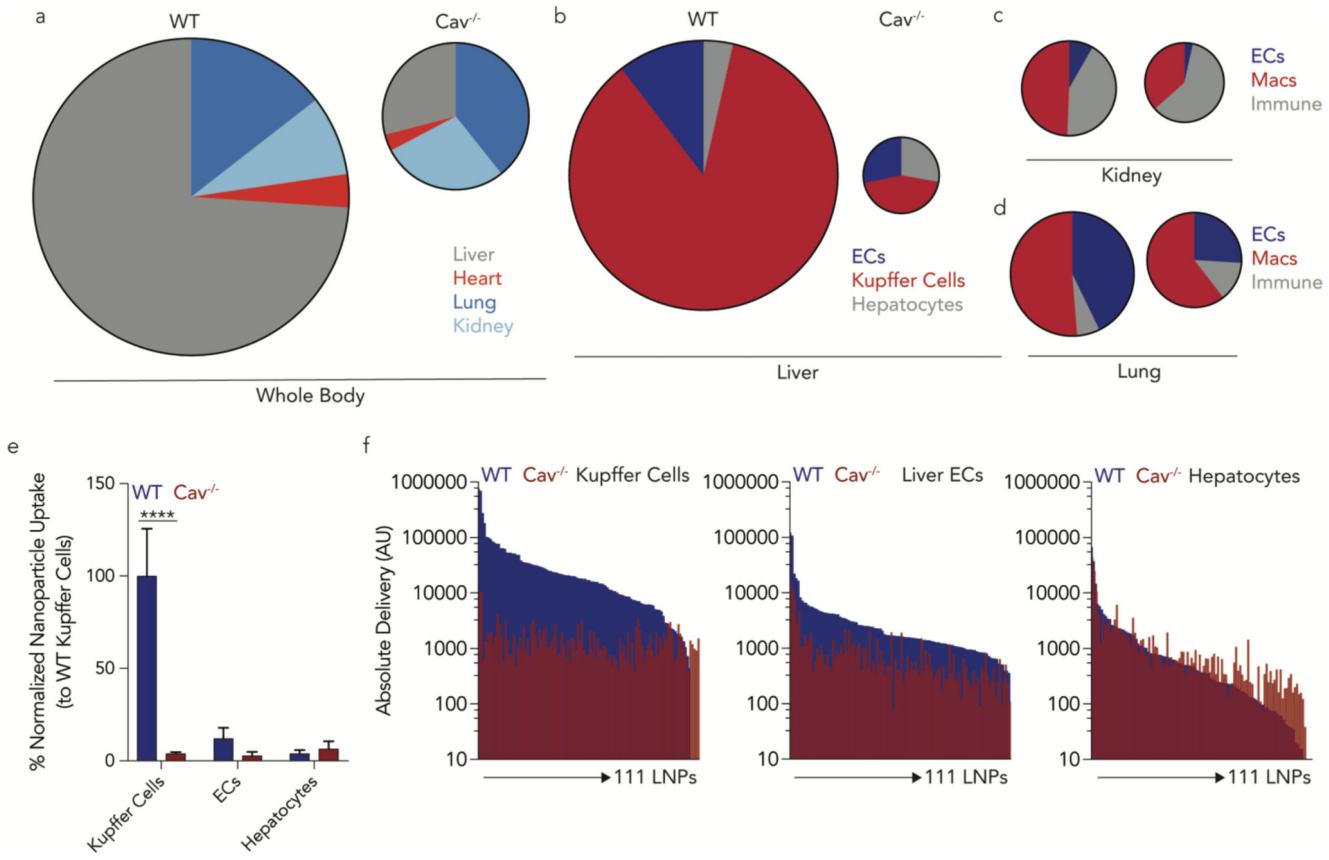

Figure 5.

High throughput QUANT studies reveal Caveolin1 affects delivery in a tissue- and cell-type dependent manner *in vivo.* **(a)** The total ddPCR counts in all tested cell types – which are equal to the area of the circle - were used to determine the 'total experimental' biodistribution in WT and Cav1$^{-/-}$ mice. **(b)** The total ddPCR counts were determined in different cell-types from the liver, **(c)** lung and **(d)** kidney. Compared to cells isolated from wild-type mice, ddPCR counts from Cav1$^{-/-}$ decreased, with the most dramatic effect in the liver. **(e)** Within the liver cell-types, normalized library 1 nanoparticle biodistribution demonstrates that Kupffer cells in Cav1$^{-/-}$ uptake less nucleic acids when compared to Kupffer cells from wild-type mice. ****$p<0.0001$ 2-way ANOVA. **(f)** Combined sequencing data and ddPCR results shows the absolute delivery of 111 nanoparticles for each LNP in the liver in wild type (blue) and Cav1$^{-/-}$ (red) mice, from library 1, in Kupffer cells, liver endothelial cells, and hepatocytes.

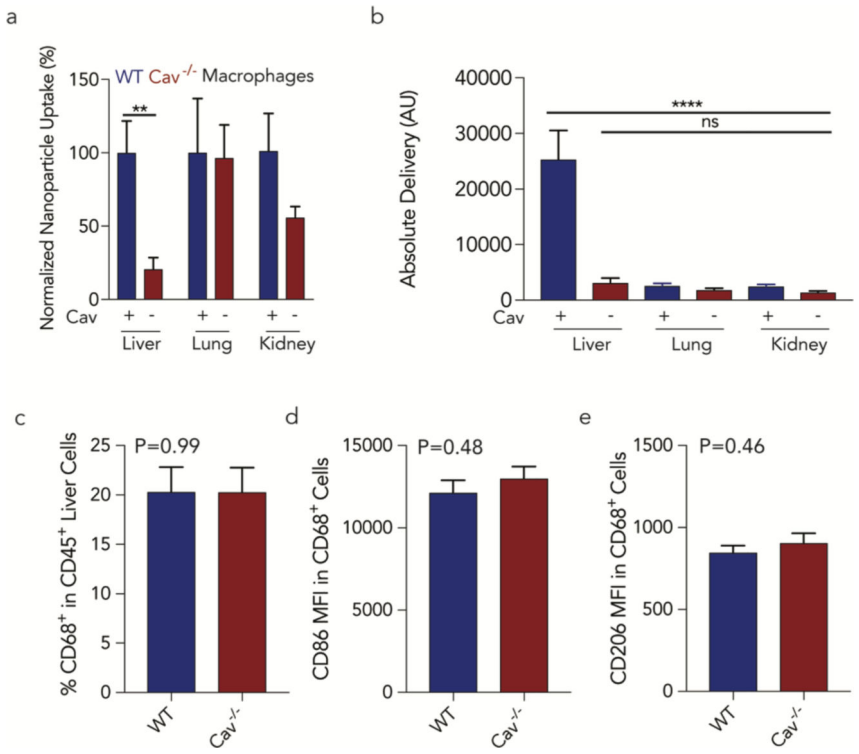

Figure 6.

Caveolin1 significantly affects delivery in Kupffer cells *in vivo.* **(a)** Nanoparticle biodistribution in macrophages were isolated from multiple tissues from wild-type and Cav1$^{-/-}$ mice. Lung and kidney macrophages were less impacted by the loss of caveolin. **p<0.01 1-tailed t-test. **(b)** Absolute nanoparticle delivery to wild-type and Cav1$^{-/-}$ macrophages in the liver, lung, and kidney. Kupffer cells were statistically significant compared to other macrophage beds. ****p<0.0001 One-way ANOVA. **(c)** The percentage of Kupffer cells (CD68^{+} CD45^{+}) within the immune cell population (CD45^{+}) in wild-type and Cav1$^{-/-}$ mice were similar. Phenotype variations in wild-type and Cav1$^{-/-}$ Kupffer (CD68^{+} CD45^{+}) cells populations were determined by MFI of **(d)** CD86 and **(e)** CD206.